

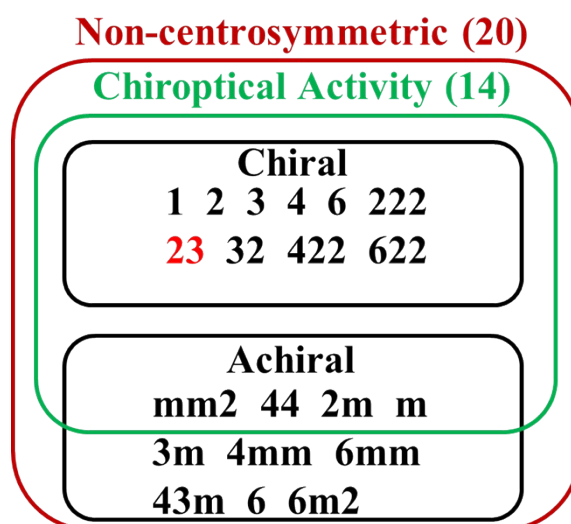
Achiral Phosphonium Induced Remarkable Circular Polarized Luminescence in Chiral Cadmium (II) Halide Perovskite Material

Shubhankar Barman,^a Priya Ranjan,^a Anuja Datta^{a,b,*}

^aSchool of Applied and Interdisciplinary Sciences, Indian Association for the Cultivation of Science, 2A and 2B Raja S. C. Mullick Road, Jadavpur, Kolkata 700 032, India.

^bTechnical Research Center, Indian Association for the Cultivation of Science, 2A and 2B Raja S. C. Mullick Road, Jadavpur, Kolkata 700 032, India.

*Corresponding Author: E-mail: psuad4@iacs.res.in



Scheme S1. Relationship between point group and chiroptical active materials. The PCC single-crystal belongs to non-centrosymmetric chiral **23 (198)** point group.

Synthesis procedure:

Chemicals: Methyltriphenylphosphonium chloride, Cadmium (II) chloride and 37% Hydrochloric acid were purchased from Sigma-Aldrich, Thermo-Fisher, and Merck. All chemicals were used without further purification.

Method: Single crystals of $(\text{MePh}_3\text{P})_2\text{CdCl}_4$ (PCC) were synthesized by the room temperature slow solvent evaporation method. $\text{MePh}_3\text{P}^+\text{Cl}^-$ (1mmol, 312.77mg) and CdCl_2 (1mmol, 183.32mg) in equal proportions were dissolved separately in a 10mL HCl (37%) and two solutions were stirred at room temperature for 30minutes. Next, $\text{MePh}_3\text{P}^+\text{Cl}^-$ solution was added slowly (drop by drop) in CdCl_2 solution under continuous magnetic stirring further 1h at room

temperature and was filtered through a thick pad of celite. A clean transparent solution was kept for crystallisation at room temperature. After 7 days, white transparent single crystals were formed. **Yield:** 76% **Melting point:** 130°C – 150°C. **³¹P NMR (162 MHz, CD₃OD):** δ 21.2

Crystallography:

The single-crystal X-ray diffraction data for PCC at 163K were obtained on a Bruker Smart Apex Duo diffractometer using Mo K α radiation ($\lambda = 0.71073 \text{ \AA}$). Crystal structures were solved using the direct method and then refined by full-matrix least-squares against F² using SHELXL-2014/7 built in the Apex 3 program and Olex2 software package.^{1,2,3} All of the non-hydrogen atoms were refined anisotropically. All hydrogen atoms were fixed in geometric positions to their parent atoms using riding model.⁴ The X-ray crystallographic structures have been deposited at the Cambridge Crystallographic Data Centre (CCDC 2233871) and can be obtained free of charge from the CCDC via <https://www.ccdc.cam.ac.uk/structures/>.

Preparation of chiral perovskite films:

The film of PCC is fabricated by drop-casting method with quartz glass as substrate. Substrate with 6mm \times 6mm dimension is washed in an ultrasonic cleaner using D.I. water, ethanol and acetone in sequence for 15 minutes each. Next, the substrate surface is dried in vacuum for 2hr. The precursor solution for the PCC is prepared by dissolving the PCC microcrystals in THF (1mmol/ml). To form the films 100 μ L of the precursor solution is spread on the quartz substrate and finally the as-fabricated film is annealed at 50°C for 30minutes on a hot-plate. The resulting 90 μ m thickness film was used for UV-VIS, PL, CD, and CPL measurements.

Physical properties measurements:

Powder XRD of PCC is measured on a Rigaku Smartlab, Hypix-3000, with CuK α radiation, $\lambda=1.5406\text{\AA}$. The diffraction data were collected in the 2 θ range 8-60° with step size 0.001°. The experimental PXRD data match fairly well with Stimulated data based on Single crystal XRD, which confirmed the pure phase of PCC (See Fig. S1). The UV-Vis absorptions in the solid-state are measured at room temperature on Optical properties were studied by a UV-Vis spectrophotometer (Agilent 8453) at rt. TGA is recorded on a Netzsch STA449C thermal analyser in the temperature range of 25°C– 600°C and recorded at heating rate of 10 K.min⁻¹. Differential scanning calorimetry (DSC) was conducted by using TA instruments (DSC Q2000). Solid-State photoluminescence (PL) spectrum was measured using a Horiba JobinYvon Fluoromax-4 spectrofluorometer.

Solid-state circular dichroism (CD) measurement: Thin film sample of PCC was used for CD measurement. Solid-state circular dichroism (CD) measurement was measured on JASCO J-810 circular dichroism spectrophotometer

Solid-state CPL measurement:

For Circularly polarized luminescence (CPL) measurements, thin film of PCC was used, film preparation as discussed earlier. The CPL-300 setup with a double prism linearly polarizing monochromator to avoid linear polarization effects, and the resultant CPL signal is free from undesired linear dichroism signals. CPL was measured by using the difference between left and right circularly polarized light intensities emitted by the sample, which was carried out with the JASCO Spectral Manager Suite supplied with the instrument. During the measurement time, digital integration time (D.I.T) was kept fixed at 4.0 sec with multiple spectral accumulations (3) at a scanning speed of 50nm.min⁻¹ to avoid noise. Sample was excited at 440nm, similar to that of fluorescence experiment and excitation/emission slit widths were maintained at 2000nm each and the instrument was calibrated with standard d-and l-camphor solutions in ethanol (0.4%WV⁻¹) prior to recording samples

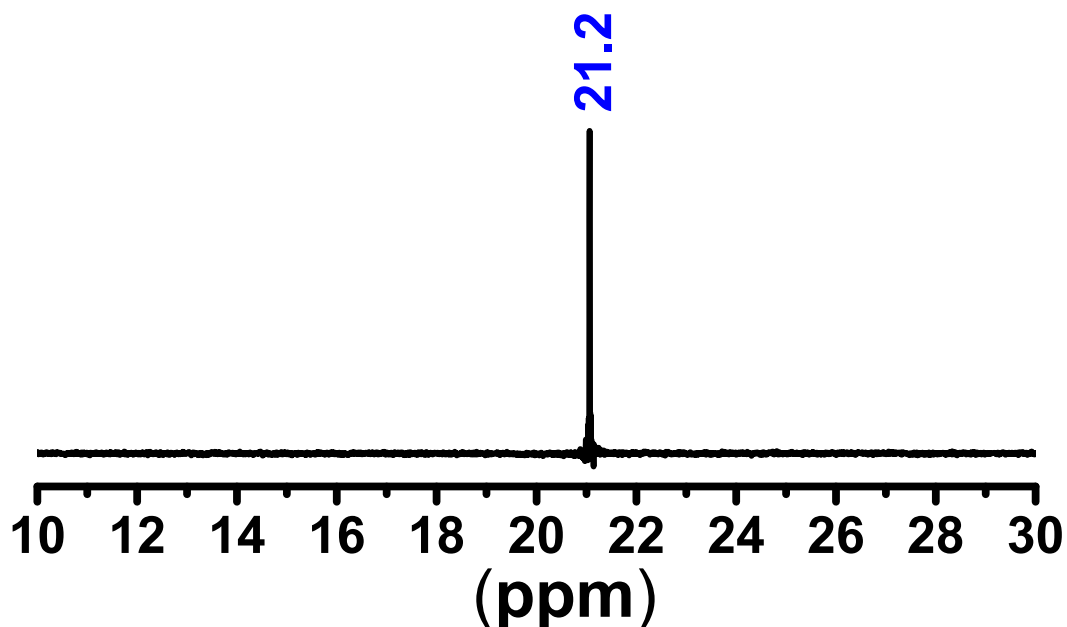


Figure S1. ³¹P NMR spectrum of PCC at room temperature.

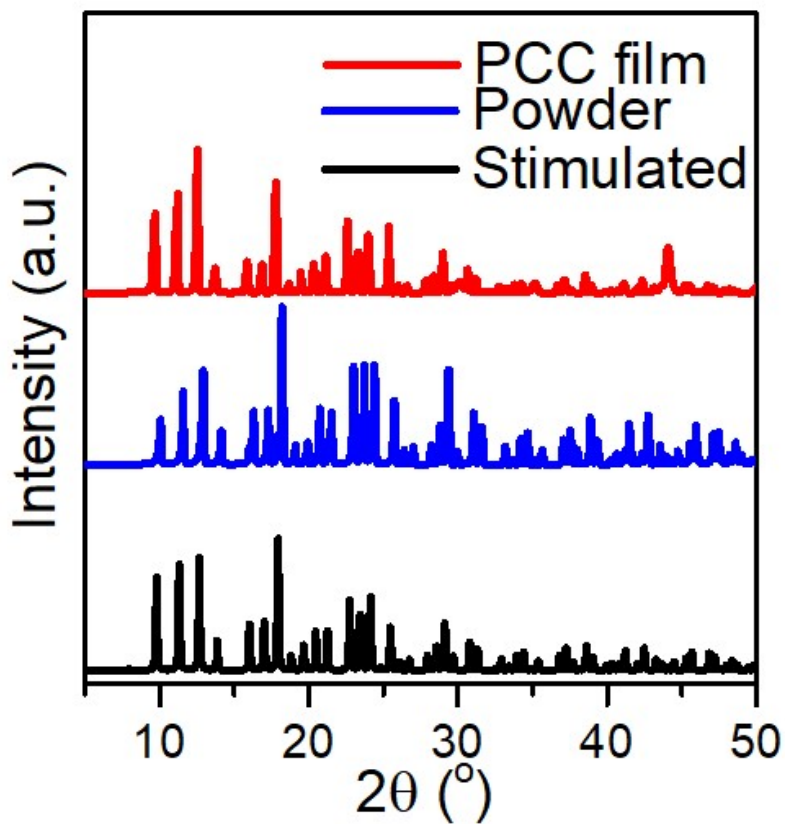
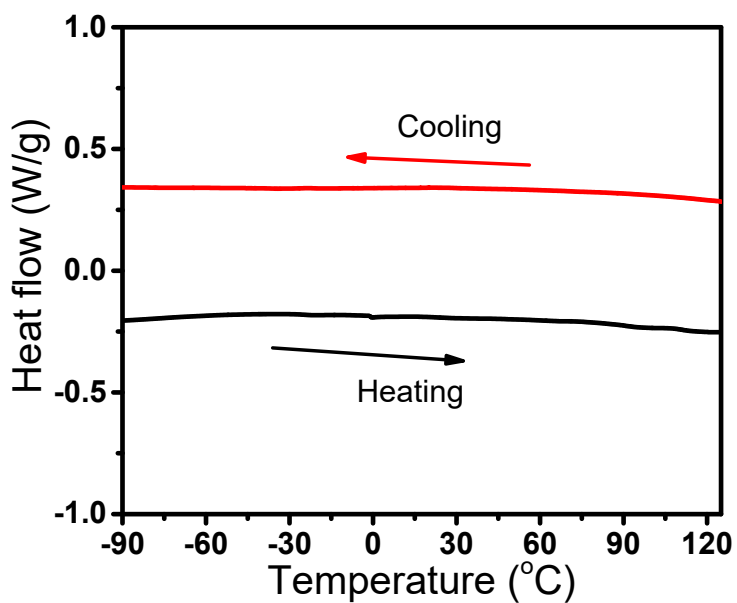


Figure S2. X-Ray diffraction patterns of PCC thin film on quartz glass, powder, and simulated. Film and powder samples are measured at room temperature, and match well with the



simulated XRD pattern.

Figure S3. Heating cooling DSC curves of PCC compound in powder form. No exothermic and endothermic peaks were observed from -90°C to 125°C.

Table 1 Crystal data and structure refinement for PCC.

Identification code	PCC	
Empirical formula	$C_{38}H_{36}CdCl_4P_2$	
Formula weight		808.81
Temperature/K		163.15
Crystal system	cubic	
Space group	P2 ₁ 3	
a/Å	15.560(15)	
b/Å	15.560(15)	
c/Å	15.560(15)	
$\alpha/^\circ$		90
$\beta/^\circ$		90
$\gamma/^\circ$		90
Volume/Å ³	3767(11)	
Z		4
$\rho_{\text{calc}}/\text{g/cm}^3$		1.426
μ/mm^{-1}		0.974
F(000)		1640
Crystal size/mm ³	0.3 × 0.1 × 0.1	
Radiation	MoK α ($\lambda = 0.71073$)	
2 Θ range for data collection/ $^\circ$	6.414 to 50.898	
Index ranges	$-18 \leq h \leq 18, -18 \leq k \leq 18, -18 \leq l \leq 17$	
Reflections collected		41861
Independent reflections	2329 [$R_{\text{int}} = 0.0320, R_{\text{sigma}} = 0.0121$]	
Data/restraints/parameters	2329/0/137	
Goodness-of-fit on F ²		1.13
Final R indexes [$I \geq 2\sigma(I)$]	$R_1 = 0.0207, wR_2 = 0.0584$	
Final R indexes [all data]	$R_1 = 0.0217, wR_2 = 0.0593$	
Largest diff. peak/hole / e Å ⁻³	0.92/-0.20	
Flack parameter	-0.02(3)	

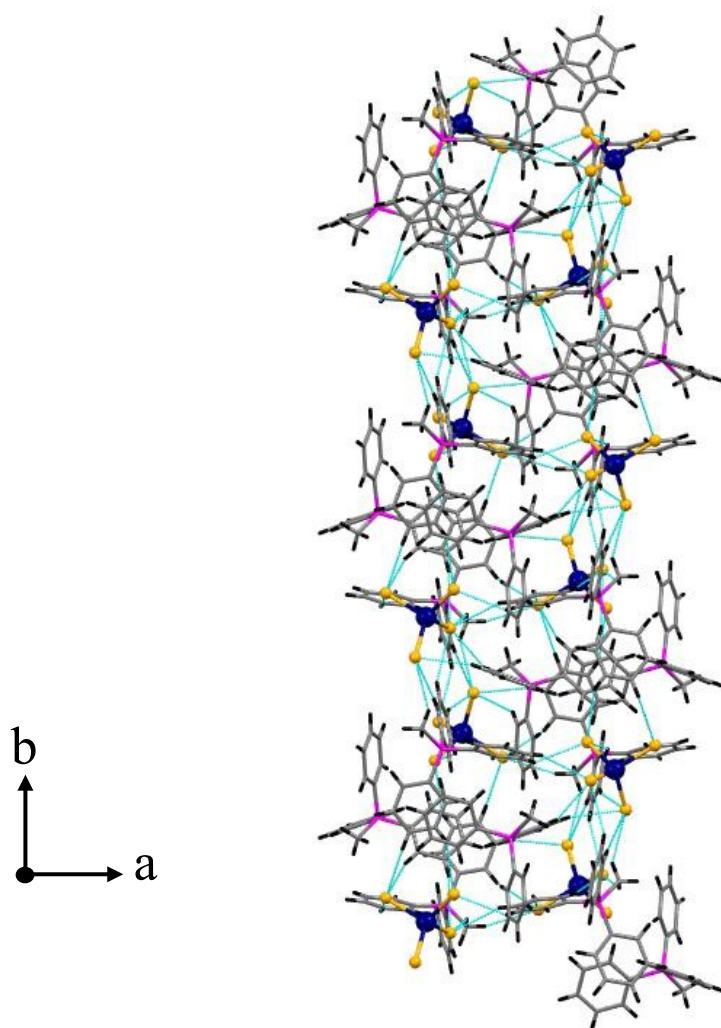
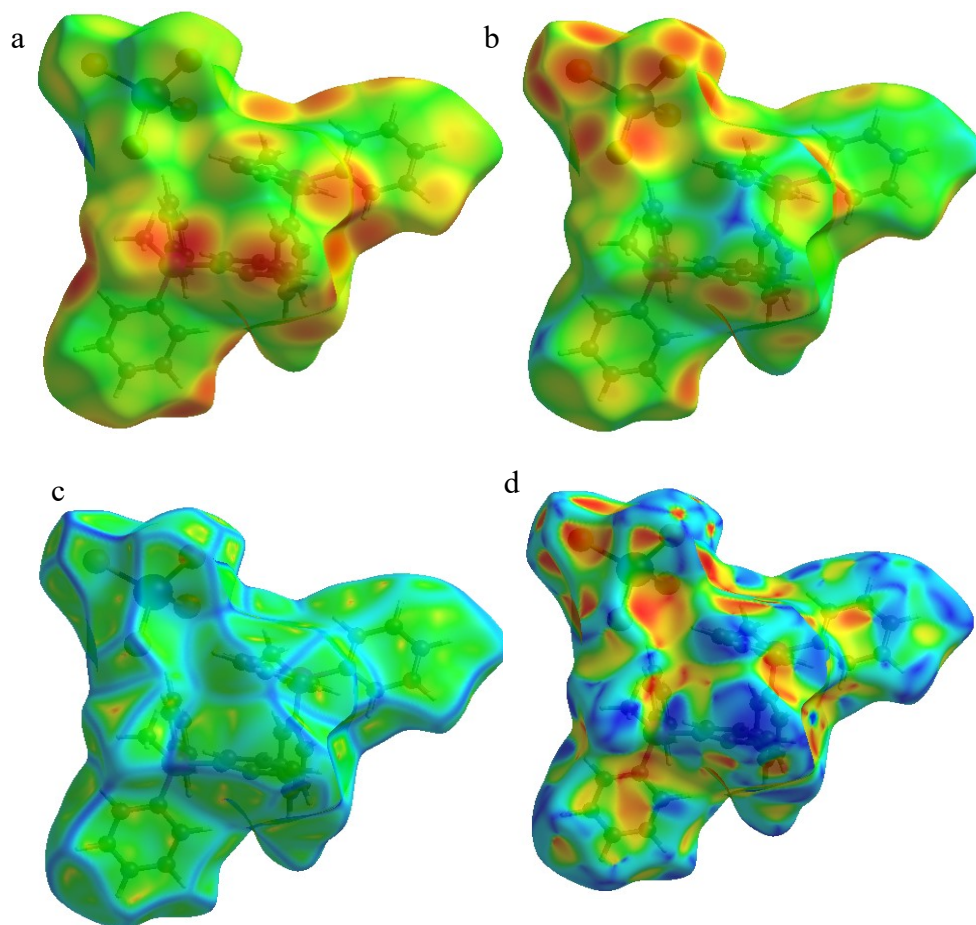


Figure S4. Cd-Cl bond distances and Cd-Cl...H hydrogen bond configuration of PCC.

PCC	Bond lengths
Cd (1)-Cl(1)	2.430(2)
Cd (1)-Cl(2)	2.461(2)
Cd (1)-Cl(2)	2.461(2)
Cd (1)-Cl(2)	2.461(2)

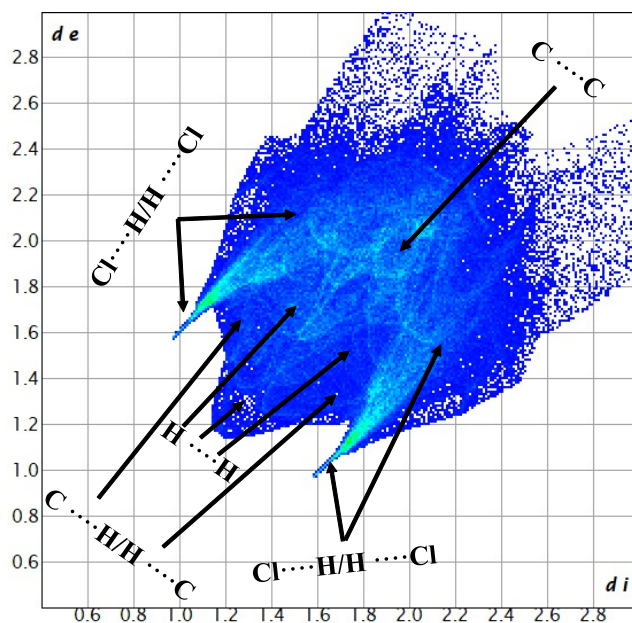
Table S2. Selected Cd-Cl bond lengths for PCC

Table S3. Selected Cd-Cl...H bond lengths for PCC



PCC	Bond lengths
Cl(2)···H(10)	2.935
Cl(2)···H(2)	2.694
Cl(2)···H(9)	2.832
Cl(2)···H(3)	2.871
Cl(2)···H(7)	2.94

Figure S5. Hirshfeld surface analysis of PCC using 3D color mapping showing (a) di, (b) de,



(c) curvedness, (d) shape index.

Figure S6. 2D fingerprint (de vs di) plot of PCC showing all the possible interactions in the molecule.

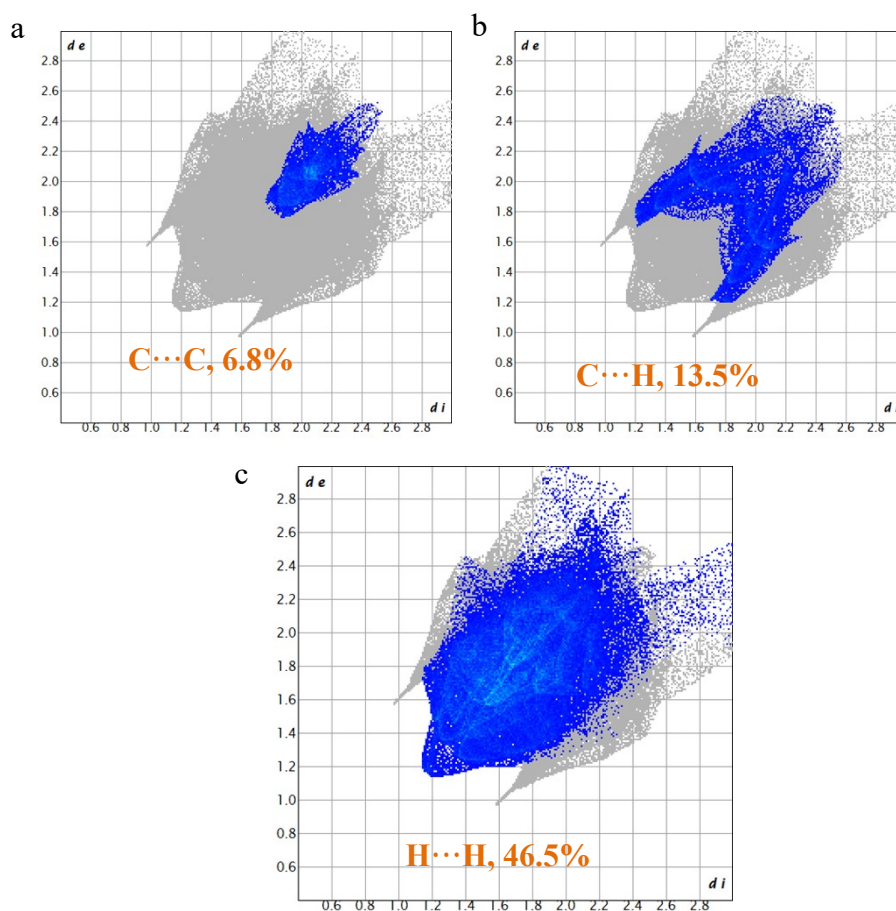


Figure S7. 2D fingerprint (de vs di) plot of PCC showing the percentages of (a) C \cdots C, (b) C \cdots H, (c) H \cdots H interactions in the molecule.

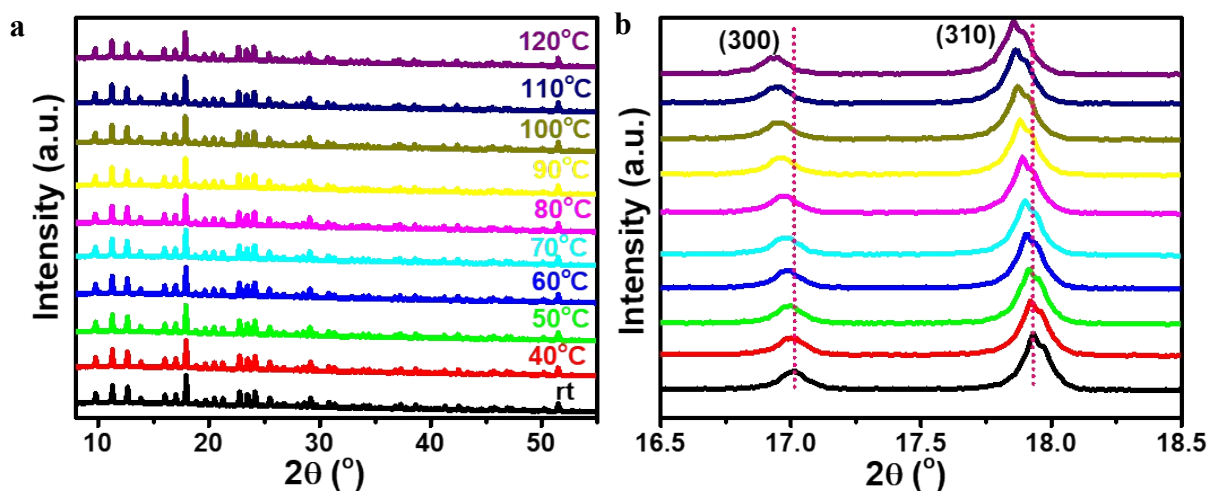


Fig. S8. (a, b) Temperature dependent powder XRD pattern of PCC compound.

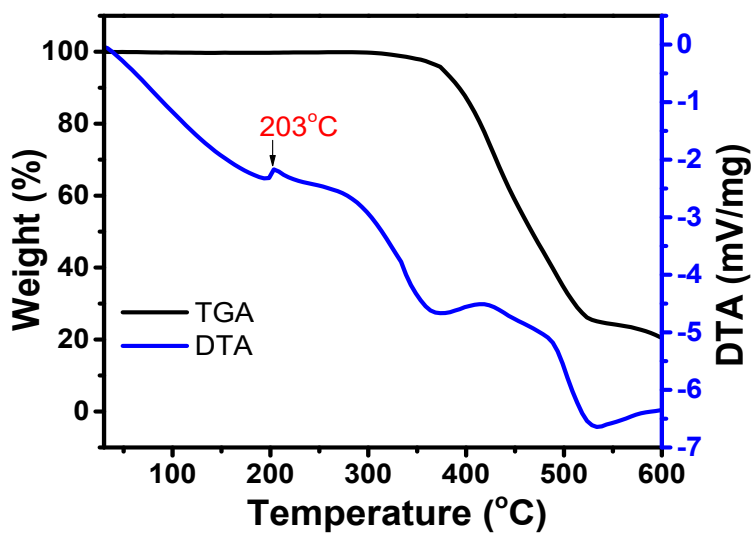


Figure S9. DTA and TGA curve of PCC compound. The result shows that PCC has a high thermal stability up to 140 degrees Celsius.

Table S4. Hirshfeld surface analysis of PCC single crystal.

Surface property	Range (Minimum/maximum)	Globularity and Asphericity	Surface volume (\AA^3) and Area (\AA^2)
d_i	0.9793 / 3.4443		
d_e	0.9791 / 3.0720		
d_{norm}	-0.1935 / 2.2577	0.724 and 0.054	930.45 and 636.34
Shape index	-0.9987 / 0.9975		
Curvedness	-3.7585 / 0.4871		

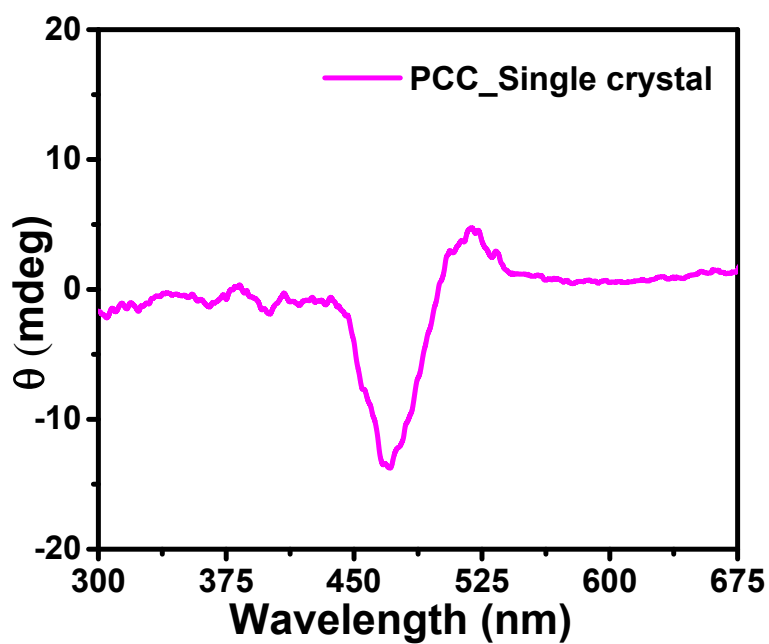


Figure S10. Circularly Dichroism (CD) spectrum of PCC single crystal at room temperature.

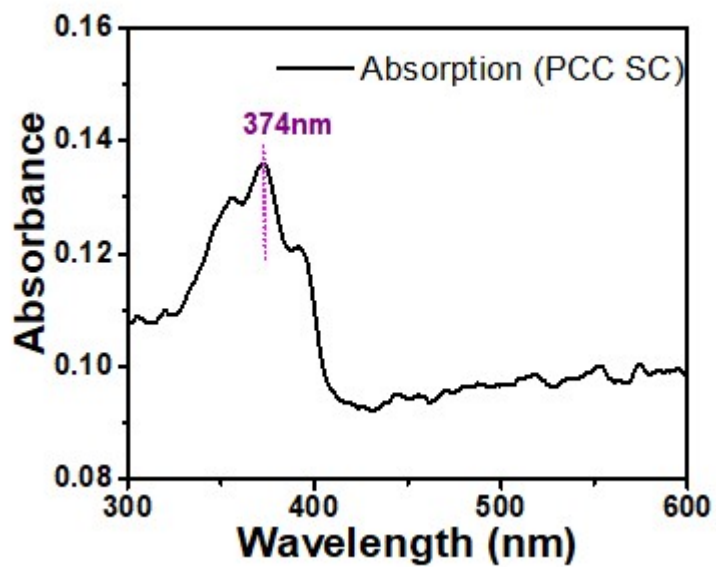


Figure S11. UV-Vis absorption spectrum of PCC single crystal shows that absorption near visible region, as compared to visible emission from PCC film.

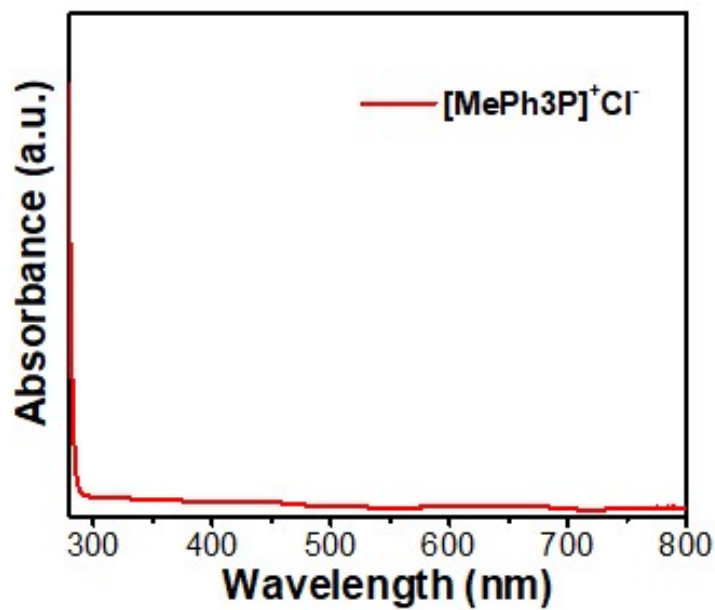


Figure S12. Solid state absorption spectrum of [MePh₃P]Cl at room temperature.

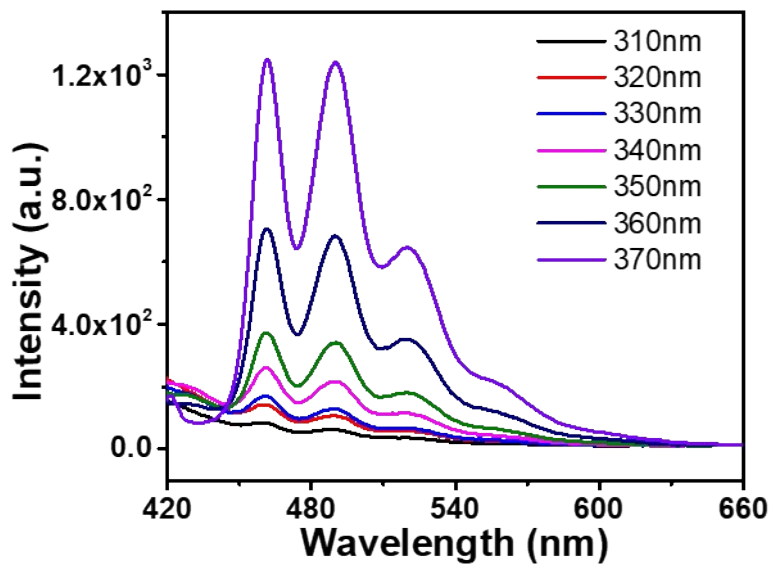


Figure S13. Excitation wavelength dependent emission spectra of PCC film at room temperature.

Table S5. Different bond angles in PCC system

Number	Atom1	Atom2	Atom3	Angle
1	C1	P1	C7	109.9(1)
2	C1	P1	C1	109.0(1)
3	C1	P1	C1	109.0(1)
4	C7	P1	C1	109.9(1)
5	C7	P1	C1	109.9(1)
6	C1	P1	C1	109.0(1)
7	H2	C2	C1	120.3
8	H2	C2	C3	120.2
9	C1	C2	C3	119.5(4)
10	P1	C1	C2	120.1(3)
11	P1	C1	C6	121.0(3)
12	C2	C1	C6	118.7(3)
13	P1	C7	H7	109.3
14	P1	C7	H7	109.3
15	P1	C7	H7	109.3
16	H7	C7	H7	109.7
17	H7	C7	H7	109.7
18	H7	C7	H7	109.7
19	C1	C6	H6	119.8
20	C1	C6	C5	120.4(4)
21	H6	C6	C5	119.8
22	H4	C4	C3	120
23	H4	C4	C5	119.7
24	C3	C4	C5	120.3(5)
25	C2	C3	C4	120.6(5)
26	C2	C3	H3	119.8
27	C4	C3	H3	119.6
28	C6	C5	C4	120.4(4)
29	C6	C5	H5	119.6
30	C4	C5	H5	119.9
31	H2	C2	C1	120.3
32	H2	C2	C3	120.2
33	C1	C2	C3	119.5(4)
34	P1	C1	C2	120.1(3)
35	P1	C1	C6	121.0(3)
36	C2	C1	C6	118.7(3)
37	C1	C6	H6	119.8
38	C1	C6	C5	120.4(4)
39	H6	C6	C5	119.8
40	H4	C4	C3	120
41	H4	C4	C5	119.7
42	C3	C4	C5	120.3(5)

43	C2	C3	C4	120.6(5)
44	C2	C3	H3	119.8
45	C4	C3	H3	119.6
46	C6	C5	C4	120.4(4)
47	C6	C5	H5	119.6
48	C4	C5	H5	119.9
49	H2	C2	C1	120.3
50	H2	C2	C3	120.2
51	C1	C2	C3	119.5(4)
52	P1	C1	C2	120.1(3)
53	P1	C1	C6	121.0(3)
54	C2	C1	C6	118.7(3)
55	C1	C6	H6	119.8
56	C1	C6	C5	120.4(4)
57	H6	C6	C5	119.8
58	H4	C4	C3	120
59	H4	C4	C5	119.7
60	C3	C4	C5	120.3(5)
61	C2	C3	C4	120.6(5)
62	C2	C3	H3	119.8
63	C4	C3	H3	119.6
64	C6	C5	C4	120.4(4)
65	C6	C5	H5	119.6
66	C4	C5	H5	119.9
67	C14	P2	C8	109.4(1)
68	C14	P2	C8	109.4(1)
69	C14	P2	C8	109.4(1)
70	C8	P2	C8	109.5(1)
71	C8	P2	C8	109.5(1)
72	C8	P2	C8	109.5(1)
73	P2	C14	H14	109.4
74	P2	C14	H14	109.4
75	P2	C14	H14	109.4
76	H14	C14	H14	109.5
77	H14	C14	H14	109.5
78	H14	C14	H14	109.5
79	H9	C9	C8	120
80	H9	C9	C10	120.1
81	C8	C9	C10	119.8(4)
82	P2	C8	C9	121.2(3)
83	P2	C8	C13	119.8(3)
84	C9	C8	C13	118.9(3)
85	C8	C13	H13	119.9
86	C8	C13	C12	120.1(3)
87	H13	C13	C12	119.9
88	C9	C10	H10	119.5
89	C9	C10	C11	120.8(5)
90	H10	C10	C11	119.7

91	C10	C11	H11	120
92	C10	C11	C12	120.0(5)
93	H11	C11	C12	120
94	C13	C12	C11	120.2(4)
95	C13	C12	H12	119.9
96	C11	C12	H12	119.9
97	H9	C9	C8	120
98	H9	C9	C10	120.1
99	C8	C9	C10	119.8(4)
100	P2	C8	C9	121.2(3)
101	P2	C8	C13	119.8(3)
102	C9	C8	C13	118.9(3)
103	C8	C13	H13	119.9
104	C8	C13	C12	120.1(3)
105	H13	C13	C12	119.9
106	C9	C10	H10	119.5
107	C9	C10	C11	120.8(5)
108	H10	C10	C11	119.7
109	C10	C11	H11	120
110	C10	C11	C12	120.0(5)
111	H11	C11	C12	120
112	C13	C12	C11	120.2(4)
113	C13	C12	H12	119.9
114	C11	C12	H12	119.9
115	H9	C9	C8	120
116	H9	C9	C10	120.1
117	C8	C9	C10	119.8(4)
118	P2	C8	C9	121.2(3)
119	P2	C8	C13	119.8(3)
120	C9	C8	C13	118.9(3)
121	C8	C13	H13	119.9
122	C8	C13	C12	120.1(3)
123	H13	C13	C12	119.9
124	C9	C10	H10	119.5
125	C9	C10	C11	120.8(5)
126	H10	C10	C11	119.7
127	C10	C11	H11	120
128	C10	C11	C12	120.0(5)
129	H11	C11	C12	120
130	C13	C12	C11	120.2(4)
131	C13	C12	H12	119.9
132	C11	C12	H12	119.9
133	C12	Cd1	C11	109.25(3)
134	C12	Cd1	C12	109.69(3)
135	C12	Cd1	C12	109.69(3)
136	C11	Cd1	C12	109.25(3)
137	C11	Cd1	C12	109.25(3)
138	C12	Cd1	C12	109.69(3)

Table S6. Summarized $|g_{CD}|$ and $|g_{lum}|$ values for other metal halide chiral materials.

Compounds	Dimension	$ g_{CD} $	$ g_{lum} $	Source of Chirality	Ref.
R- $Cu_2I_2(BINAP)_2^a$	0D	-	0.005	Chiral chelating ligand	5
S- $Cu_2I_2(BINAP)_2$	0D	-	0.005	Chiral chelating ligand	5
inorganic perovskite nanoplatelets (NPLs)	-	0.0008	0.0023	Chiral organic cation	6
$CsPbBr_3$	-	0.0062	0.006	Inorganic silica right (or left) handed nanohelices	7
(R/ S-MBA) SbI_4^b	1D	0.02	Inactive	Chiral organic cation	8
(R-XH ⁺) $MnBr_3^c$	1D	0.0137	0.023	Chiral organic cation	9
(S-XH ⁺) $MnBr_3$	1D	0.0105	0.0227	Chiral organic cation	9
(R-YH ⁺) $MnBr_3^d$	1D	0.0072	0.0191	Chiral organic cation	9
(S-YH ⁺) $MnBr_3$	1D	0.0117	0.0159	Chiral organic cation	9
(R-DMPZ) $PbBr^e$	1D	0.0000 46	0.021	Chiral organic cation	10
(S-DMPZ) $PbBr_4$	1D	0.0003 5	0.0232	Chiral organic cation	10
(D-TBP) $MnCl_3^f$	1D	-	0.0061	Chiral organic cation	11
(L-TBP) $MnCl_3$	1D	-	0.0061	Chiral organic cation	11
(R- $C_6H_{16}N_2$) $PbBr$	2D	-	0.002	Chiral organic cation	12
(S- $C_6H_{16}N_2$) $PbBr_4$	2D	-	0.002	Chiral organic cation	12
(R- BrMBA) $_2PbI_4^g$	2D	-	0.002	Chiral organic cation	13
(R-FMBA) $_2PbI_4^h$	2D	-	0.0003	Chiral organic cation	13
[(S/R)-MBABr] + $PbBr_2$ + (FABr) ⁱ	Thin film	0.004	0.004	Chiral organic cation	14
R-MPEA, S- MPEA perovskite Nanosheets ^j	2D	0.006	-	Intrinsic	15
R-Pero-NCs, S-Pero-NCs	-	0.0023, 0.0024	0.0065, 0.001	Molecular chirality of the capping ligands	16
PCC, (MePh₃P)₂CdCl₄	2D	0.005	0.043	Intrinsic	work

a) BINAP, 2,2-bis(diphenylphosphino)-1,1-binaphthalene; b) R/S-MBA, R- and S-methylbenzylammonium; c) X, 3-quinuclidinol; d) Y, 2-amino-1-propanol; e) DMPZ, cis-2,5-dimethylpiperazine divalent cation; f) TBP, tert-butyl prolinatate; g) BrMBA, (4-bromophenyl)ethan ammonium; h) FMBA, (4-fluorophenyl)ethan ammonium; i) (S/R)-MBABr, (S/R)-(+)- α -methylbenzylammonium bromide; FABr, formamidinium bromide; j) MPEA, β -methylphenethylamine.

References

1. G. M. Sheldrick, *Acta Cryst.*, 2008, **A64**, 112.
2. O. V. Dolomanov, L. J. Bourhis, R. J. Gildea, J. A. K. Howard, H. Puschmann, *J. Appl. Cryst.* 2009, **42**, 339.
3. L. J. Bourhis, O. V. Dolomanov, R. J. Gildea, J. A. K. Howard, H. Puschmann, H., *Acta Cryst.*, 2015, **A71**, 59.
4. A. L. Spek, *Acta Cryst.*, 2009, **D65**,148.
5. J. J. Wang, H. T. Zhou, J. N. Yang, L. Z. Feng, J. S. Yao, K. H. Song, M. M. Zhou, S. Jin, G. Zhang, and H. B. Yao, *J. Am. Chem. Soc.* 2021, **143**, 10860.
6. Q. Cao, R. Song, C. C. S. Chan, Z. Wang, P. Y. Wong, K. S. Wong, V. Blum, H. Lu, *Adv. Optical Mater.* 2023, 2203125.
7. P. Liu, W. Chen, Y. Okazaki, Y. Battie, L. Brocard, M. Decossas, E. Pouget, P. M. Buschbaum, B. Kauffmann, S. Pathan, T. Sagawa, and R. Oda, *Nano Lett.* 2020, **20**, 8453.
8. L. Yao, K. H. Xue, H. Tong, C. Chen, G. Niu, W. Yang, and J. Tang, *Cryst. Growth Des.* 2022, **22**, 5552.
9. J. Chen, S. Zhang, X. Pan, R. Li, S. Ye, A. K. Cheetham, L. Mao, *Angew. Chem. Int. Ed.* 2022, **61**, e202205906.
10. C. Y. Chai, Q. K. Zhang, C. Q. Jing, X. B. Han, C. D. Liu, B. D. Liang, C. C. Fan, Z. Chen, X. W. Lei, A. Stroppa, R. O. Agbaoye, G. A. Adebayo, C. F. Zhang, W. Zhang, *Adv. Optical Mater.* 2023, **11**, 2201996.
11. H. L. Xuan, Y. F. Sang, L. J. Xu, D. S. Zheng, C. M. Shi, Z. N. Chen, *Chem. - Eur. J.* 2022, **28**, e202201299.
12. X. H. Zhao, X. Hu, M. E. Sun, X. M. Luo, C. Zhang, G. S. Chen, X. Y. Dong and S. Q. Zang, *J. Mater. Chem. C* 2022, **10**, 3440.
13. J. T. Lin, D. G. Chen, L. S. Yang, T. C. Lin, Y. H. Liu, Y. C. Chao, P. T. Chou, C. W. Chiu, *Angew. Chem., Int. Ed.* 2021, **133**, 21604.
14. L. Tao, H. Zhan, Y. Cheng, C. Qin, L. Wang, *J. Phys. Chem. Lett.* 2023, **14**, 2317.
15. H. Ren, Y. Wu, C. Wang, Y. Yan, *J. Phys. Chem. Lett.* 2021, **12**, 2676.
16. W. Chen, S. Zhang, M. Zhou, T. Zhao, X. Qin, X. Liu, M. Liu, P. Duan, *J. Phys. Chem. Lett.* 2019, **10**, 3290.